IET Radar, Sonar & Navigation

Research Article

IET Journals
The Institution of Engineering and Technology

Evaluation of rodents' respiratory activity using a bioradar

ISSN 1751-8784
Received on 18th December 2014
Revised on 25th June 2015
Accepted on 6th July 2015
doi: 10.1049/iet-rsn.2014.0553
www.ietdl.org

Lesya Anishchenko[1] ✉, Gianluca Gennarelli[2], Alexander Tataraidze[1], Ekatherina Gaysina[1], Francesco Soldovieri[2], Sergey Ivashov[1]

[1]*Remote Sensing Laboratory, Bauman Moscow State Technical University, 2nd Baumanskaya 5, Moscow 105005, Russia*
[2]*Institute for Electromagnetic Sensing of the Environment, National Research Council of Italy, Via Diocleziano 328, 80124, Naples, Italy*
✉ *E-mail: anishchenko@rslab.ru*

Abstract: The estimation of breathing activity of laboratory animals after drug administration attracts considerable interest in the context of the pharmacological experimentation. So far, this task has been mostly accomplished by means of expensive and cumbersome procedures requiring the application of sensors on the animal body. In this study, the authors present a feasibility study on the possible usage of bioradar devices for contactless monitoring the respiratory rhythm of living rodents. Experiments are performed in laboratory conditions on sleeping rats by using a continuous wave Doppler radar operating at 13.8 GHz. The recorded signals are processed by means of a data processing strategy, based on a novel motion artefacts filtering procedure, with the final aim to characterise the breathing pattern variability during the sleep phases. The achieved results are consistent with biological information available from the literature confirming the potential application of bioradiolocation instead of standard on-body monitoring methods.

1 Introduction

Continuous wave (CW) Doppler radars or simply 'bioradars' for contactless detection and monitoring of respiratory and heartbeat activity are known since 1970s [1, 2]. Their basic working principle relies on the fact that an electromagnetic wave reflected by a periodically moving surface is characterised by a phase modulation, which can be related to the periodic displacement.

Nowadays, also thanks to the significant technological advances, bioradar devices turn out to be an interesting tools in several applicative areas such as military, security, and healthcare. Representative military applications are the battlefield triage [3] and the localisation of terrorists and hostages inside the buildings during counter-terrorism operations [4, 5]. Another popular usage is in disaster medicine, where bioradars can support the detection of humans under the debris of destroyed buildings after natural disasters [6, 7].

As regards security applications, an interesting example is concerned with the border surveillance: in fact, transport containers can be examined for revealing hidden persons [4]. Additionally, the remote speech detection [8] and diagnostics of psycho-emotional state during latent or open checks in criminal investigations or at checkpoints [4] can be also accomplished via bioradars.

Another major application area of bioradar is related to healthcare. Contactless registration of heartbeat and breathing parameters is crucial in the case of burnt patients and more in general patients where on-body sensors cannot be used [4, 5, 9]. In sleep medicine, bioradars allow monitoring the respiration and heartbeat pattern during night sleep in order to diagnose sleep apnea syndrome [10, 11]. With regard to newborns, it is possible to exploit bioradiolocation to prevent the sudden infant death syndrome [12], by generating an alarm signals when no breathing activity is observed within a given time interval. Bioradars also permit to estimate the vessel elasticity from pulse-wave velocity for revealing patients predisposed to cardiovascular diseases [13]. Other application examples are the tumour tracking in radiation therapy [12] and the imaging of cardiac motion [14]. Finally, bioradars are of interest for the development of smart homes for monitoring the movements of elderly subjects [12].

However, not only human vital signs can be monitored by Doppler radars but also, these devices may be also employed in pharmacology and zoo-psychology for the study of new medicines or when conducting behavioural tests for measuring the loco-motor activity of rodents [15, 16], and for monitoring the breathing pattern to distinguish between different sleep stages [17].

The goal of the present work is to carry out a feasibility study of Doppler radars usage for monitoring the breathing pattern of sleeping rodents. This method is helpful to record the respiration pattern after the administration of new medicines and when testing new approaches for treating different sleep disorders. At present, invasive and contact methods are used to control the physiological parameters of laboratory animals. The main drawback of invasive methods is the high workload and time consumption because of the necessity to implant electrodes (on-body sensor). Specifically, for measurements of animal breathing pattern, perimetric belts and nasal cannulas are applied similar to those used for humans. However, these methods provide reliable results only when the animal motion is restrained.

Standard clinical devices for full-body plethysmography for a contactless estimation of animals' respiration parameters are available on the market [18–20]. However, these devices are not free from drawbacks, and are mostly related to suitability for a specific animal and high cost. Accordingly, a completely contactless and low-cost method for prolonged monitoring of sleeping animal breathing pattern, which can be applied for different types of animals, has a high practical value.

As a main contribution, this work demonstrates the possibility to monitor the breathing pattern of living rodents for the detection and characterisation of sleep breathing disorder episodes; this goal is achieved by means of an *ad-hoc* developed data processing approach by exploiting a novel motion artefact removal procedure.

Therefore, the paper is organised as follows. An overview of CW Doppler radar is provided in Section 2. Section 3 deals with the description of the radar system and of the measurement set-up adopted for the experiments. Section 4 is concerned with the signal processing strategy exploited to extract the useful information from recorded data. Experimental results are reported in Section 5 and conclusions follow in Section 6.

2 Overview of CW Doppler radars

The general architecture of the CW Doppler radar is depicted in Fig. 1. In its basic operation, the transmitter generates an unmodulated signal $X_T(t) = A_t \cos(2\pi ft + \Psi(t))$, where A_t is the amplitude, f is the frequency, and $\Psi(t)$ is the phase. The electromagnetic signal radiated in the environment is reflected by the target, that is, the rodent, whose surface is characterised by tiny and periodic physiological movements related to breathing and cardiac activity. If $d(t) = d_0 + p(t)$is the distance between the radar and the target (d_0 is the nominal distance and $p(t)$ is the periodic displacement), the signal at the terminals of the receiving antenna is given by

$$X_R(t) = A_r \cos\left(2\pi ft - \frac{4\pi d_0}{\lambda} - \frac{4\pi p(t)}{\lambda} + \Psi\left(t - \frac{2d(t)}{c}\right)\right) \quad (1)$$

in which A_r is the signal amplitude accounting for two-way propagation, target cross-section, and antenna effects. $\lambda = c/f$ is the propagating wavelength in free space and c is the speed of light.

The received signal is down converted to baseband by exploiting as a local oscillator a reference signal derived from the transmitted signal $X_T(t)$. Upon neglecting inessential amplitude terms, the baseband signal at the output of the amplifier reads as

$$S(t) \simeq \cos\left(\alpha + \frac{4\pi p(t)}{\lambda} + \Delta\Psi(t)\right) \quad (2)$$

with $\alpha = 4\pi d_0/\lambda$, and $\Delta\Psi(t) = \Psi(t) - \Psi(t - (2d(t)/c))$ being a residual phase noise. The above expression highlights the non-linear (phase) modulation effect induced by the physiological movement on the radar echo.

In the case of a single-tone periodic displacement $p(t)$ with frequency f_p, the baseband output $S(t)$ can be expressed as the superposition of Fourier harmonics of the fundamental frequency f_p [21]. Therefore, it is sufficient to evaluate the fundamental frequency of the spectrum of $S(t)$ to estimate the frequency of the vital parameter of interest. However, according to (2), the detection sensitivity significantly depends on the nominal distance d_0 (in relation to λ) from the radar, which can result in an optimal or null detection point [21]. In particular, when α is an odd integer multiple of $\pi/2$ the maximum sensitivity is achieved, while values of α that are even integer multiples of $\pi/2$ yield the worse sensitivity.

To improve the detection performance, quadrature Doppler radars have been proposed [22]. In this case, the radar receiver has two separate channels, that is, the I (in-phase) and Q (quadrature) channels. The corresponding baseband outputs are given by

$$I(t) \simeq \cos\left(\alpha + \frac{4\pi p(t)}{\lambda} + \Delta\Psi(t)\right) \quad (3)$$

$$Q(t) \simeq \sin\left(\alpha + \frac{4\pi p(t)}{\lambda} + \Delta\Psi(t)\right) \quad (4)$$

According to (3) and (4), when $I(t)$ is at an optimal detection point $Q(t)$ is at null detection point and vice versa. Under these conditions, there is always one channel that ensures the best sensitivity. For that reason, the I/Q channel selection has been proposed as a way to improve the detection sensitivity [22]. On the other hand, when α is an integer multiple of $\pi/4$ neither $I(t)$ nor $Q(t)$ is close to an optimal detection point and a reliable estimation can be done only provided that the displacement is small compared with λ [21].

Robust and automatic detection schemes that do not require selecting one between the I and Q channels but exploit both signals simultaneously have been devised. These are the complex linear demodulation [12] and non-linear arc-tangent demodulation [23].

In complex linear demodulation, the baseband signals are combined as

$$Z(t) = I(t) + \mathrm{j}\, Q(t) = \mathrm{e}^{\mathrm{j}\left(\alpha + \frac{4\pi p(t)}{\lambda} + \Delta\Psi(t)\right)} \quad (5)$$

Unlike the single signal $I(t)$ or $Q(t)$, the amplitude of the Fourier harmonics of the complex signal $Z(t)$ is not affected by the null point detection problem (sensitivity not dependent on distance d).

Arctangent demodulation is based on the evaluation of the arctangent of the ratio between $Q(t)$ and $I(t)$, that is

$$\phi(t) = \tan^{-1}\left(\frac{Q(t)}{I(t)}\right) = \alpha + \frac{4\pi p(t)}{\lambda} + \Delta\Psi(t) \quad (6)$$

After removing the phase discontinuities related to the crossing between adjacent quadrants, the phase $\phi(t)$ in (6) is directly proportional to the signal $p(t)$. This method is very useful since it allows compensating for the non-linearity related to the phase modulation. However, its application is not easy in real-life operating conditions because it necessitates an accurate calibration of the DC offsets to provide accurate angular information. The DC offsets are produced not only by hardware but also from stationary objects and stationary parts of the target. As a result, repeated calibrations must be performed in response to changes in the environment [12].

3 System description and measurement set-up

For the present study, we have used the multifrequency Doppler radar BioRASCAN-14 (see Fig. 2), which is based on a quadrature receiver designed at Remote Sensing Laboratory of the Bauman Moscow State Technical University. The main technical parameters of the system are summarised in Table 1. The radar operates by emitting and recording CW data in the frequency range [13.8, 14.2] GHz. Two co-located standard gain horn antennas are adopted to transmit and receive the electromagnetic signal.

According to the data reported in Table 1, the maximum power density radiated by the radar is equal to 1.36 μW/cm^2. Such a value satisfies the Russian standard for microwave emission, which is 25 μW/cm^2 in the frequency range [3–300] GHz (for 24 h exposure). Moreover, the maximum field level of 3.2 V/m is

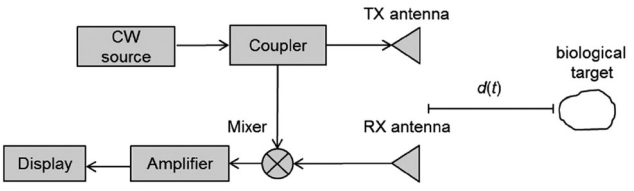

Fig. 1 *Basic architecture of the CW Doppler radar for bioradiolocation*

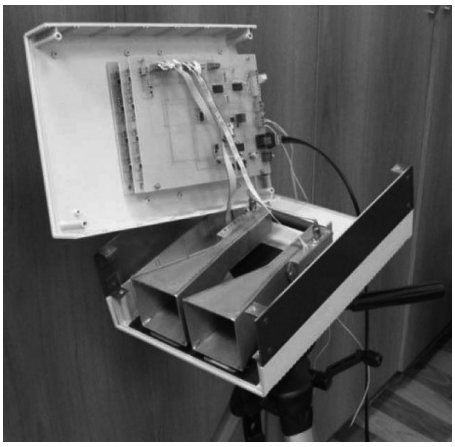

Fig. 2 *Photo of the unassembled Doppler radar BioRASCAN-14*

Table 1 Parameters of BioRASCAN-14

no. of frequencies	8
frequency range, GHz	13.8–14.2
modulation type	stepped frequency
maximum radiated power density, $\mu W/cm^2$	1.36
maximum field level, V/m	3.2
dynamic range, dB	60
analogue bandwidth, Hz	10
sampling rate, Hz	100
range resolution, m	0.375
antenna gain, dB	7

lower than guideline value of 41.2 V/m recommended by the World Health Organisation, International Commission on Non-Ionizing Radiation Protection and European Union [24], and also lower than the more severe limits adopted by several European governments (e.g. 6 V/m for an exposure of 4 h or more in Italy).

During the experiments, the radar unit was located at the distance of 0.3 m from a plastic box containing a sleeping rat as shown in Fig. 3. Such a short distance was chosen because of the relatively small scattering cross-section of the rat. Since the range of the target is not required for the estimation of the breathing activity, a single probing frequency mode was chosen at the frequency of 13.8 GHz.

Two female rats (four months old each) were used for the experiments. From each of them, five records of the received radar signals were collected, where the duration of every record was not <30 min. Besides the main goal of demonstrating the feasibility of breathing pattern detection, the other goal of the experiment was to analyse the differences in the respiratory activity of the two rats.

4 Data processing approach

In this section, we describe the approach developed to process the signals recoded by the radar system BioRASCAN-14. It is worthwhile to stress that the data processing plays a fundamental role to achieve a reliable estimation of breathing activity. As will be shown, the raw signals are typically characterised by spurious artefacts arising when animal motion is not negligible in terms of the probing wavelength. The scheme summarising the various steps of the signal processing chain is depicted in Fig. 4.

The first stage deals with the automatic selection of the best baseband signal over the I and Q channels. This task is performed by considering the component with higher peak-to-peak variation, after an average removal operation. The reason for performing I/Q channel selection instead of combining both signals according to linear or arctangent demodulation is mainly related to its simplicity. Indeed, in this specific case, the detection sensitivity is satisfactory because the physiological movements associated with the respiratory activity of rats are small compared with the probing wavelength.

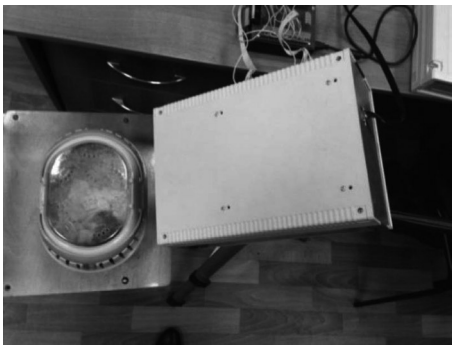

Fig. 3 *Photo of the experimental set-up*

The second processing step consists in a band-pass filtering of the radar signal [see (3) or (4)], in order to remove high-frequency (with respect to the useful signal) noise and very low-frequency fluctuations. To this end, a third-order Butterworth filter with bandwidth [0.3, 3.0] Hz is applied.

After filtration, a thresholding procedure is developed to ensure an adequate rejection of motion artefacts. As stated, sudden movements of the rat during sleep produce spurious signals localised in time, whose amplitude is generally much higher than the useful breathing signal. In such time intervals, the breathing pattern cannot be reliably estimated. The objective of the artefact removal procedure is to reject automatically the corrupted parts of the signal, while keeping as much as possible unaltered the uncorrupted ones. The artefact removal procedure here proposed can be summarised as follows.

Let $Y(t)$ be the signal at the output of the filtering block (see Fig. 4) and denote with $Y(n)$, $n = 1, \ldots, N$ its discrete-time version, with N being the total number of samples. Let $M < N$ denote the length of a window function $w(n)$. The one-dimensional (1D) time series $Y(n)$ is first transformed into a multidimensional sequence of lagged vectors. This embedding operation is performed by the window $w(n)$. In particular, starting from $n = 0$, the lagged vectors are composed by the M signal samples falling within the window $w(n)$, which is progressively translated forwards of one sample up to the last sample in the sequence $Y(n)$. In this way the following trajectory matrix is constructed

$$\boldsymbol{Y} = \begin{bmatrix} Y(M-1) & Y(M) & \cdots & Y(N-1) \\ Y(M-2) & Y(M-1) & \cdots & Y(N-2) \\ \vdots & \vdots & \ddots & \vdots \\ Y(0) & Y(1) & \ldots & Y(N-M) \end{bmatrix} \tag{7}$$

The matrix $\boldsymbol{Y}$ has M rows and $K = N - M + 1$ columns. Moreover, it has Toeplitz structure, that is, equal elements along the diagonals. It is timely to remark that the representation of a 1D time series in terms of a trajectory matrix usually represents the starting point of singular spectrum analysis methods [25].

After that, we evaluate the squared norm of each column in the matrix $\boldsymbol{Y}$, that is, the energy of the original signal in time-delayed coordinates

$$\varepsilon(k) = \sum_{m=0}^{M-1} Y^2(m, k), \qquad k = 0, \ldots, K-1 \tag{8}$$

It is intuitively clear that the function $\varepsilon(k)$ assumes high values for indexes k corresponding to time intervals containing motion artefacts. On the other hand, intervals corresponding to low values of $\varepsilon(k)$ contain only the useful respiratory signal. This consideration suggests estimating the artefact-free trajectory matrix

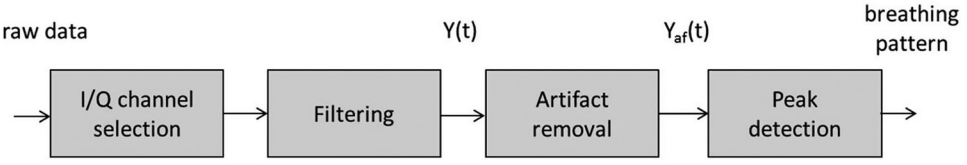

Fig. 4 *Block diagram of the processing strategy for the estimation of the breathing pattern*

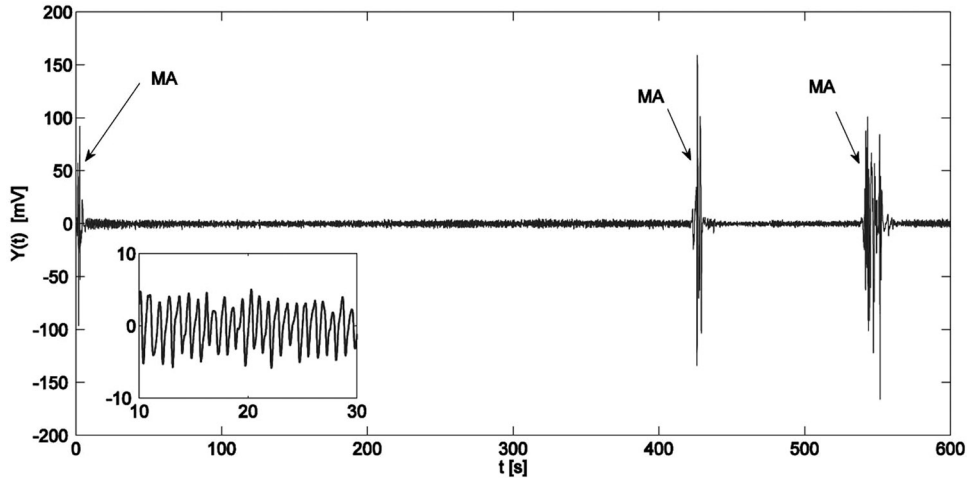

Fig. 5 *Recorded signal at the output of the low-pass filter over the time window [0, 600] s for rat 1. The inset shows the signal over the interval [10, 30] s, while black arrows denote motion artefacts*

$\tilde{\boldsymbol{Y}}$ with entries evaluated according to the following thresholding rule

$$\tilde{Y}(m,k)=\begin{cases}0, & \varepsilon(k)>\tau,\\ Y(m,k), & \varepsilon(k)<\tau,\end{cases} \qquad m=0,\ \ldots,M-1,\quad k=0,\ \ldots,K-1 \tag{9}$$

The threshold value τ is here chosen on the basis of the average value of the signal energy in time-delayed coordinates, that is

$$\tau=\varepsilon_{\mathrm{av}}=\frac{1}{K}\sum_{k=0}^{K-1}\varepsilon(k) \tag{10}$$

Such a simple criterion is justified since motion artefact signals are localised in time and typically have a significantly higher intensity than breathing signal. Hence $\varepsilon(k)$ is expected to be always lower than $\varepsilon_{\mathrm{av}}$ save for time intervals containing motion artefacts.

After the artefact-free trajectory matrix $\tilde{\boldsymbol{Y}}$ is computed, the final step of the artefact removal procedure is a diagonal averaging operation that consists of replacing the entries of each diagonal of $\tilde{\boldsymbol{Y}}$ by their average. This operation is necessary to restore the original Toeplitz structure, which is typically no more available after the thresholding operation. In this way, a new trajectory matrix $\tilde{\boldsymbol{Y}}_{\mathrm{d}}$ is obtained. Finally, the time-domain artefact-free signal $Y_{\mathrm{af}}(t)$ is recovered by reverting the embedding operation. This task is easily performed by taking a sample in each diagonal of $\tilde{\boldsymbol{Y}}_{\mathrm{d}}$[25].

According to the block diagram in Fig. 4, the final stage of the signal processing is concerned with the estimation of peak locations in the signal $Y_{\mathrm{af}}(t)$. The whole data processing software has been implemented in the MATLAB environment.

5 Experimental results

In this section, we show the results of the experimental tests carried out to assess the effectiveness of bioradiolocation for monitoring the breathing activity of two sleeping rats (rat 1 and rat 2). It is also interesting to analyse the outputs at the various stages of the processing chain displayed in Fig. 4.

The curve plotted in Fig. 5 refers to rat 1 and shows the signal $Y(t)$ at the output of the low-pass filter over the time window [0, 600] s. The inset in the figure depicts the same signal over the interval [10, 30] s, which clearly exhibits an almost periodical behaviour related to the breathing activity with the exception of the intervals

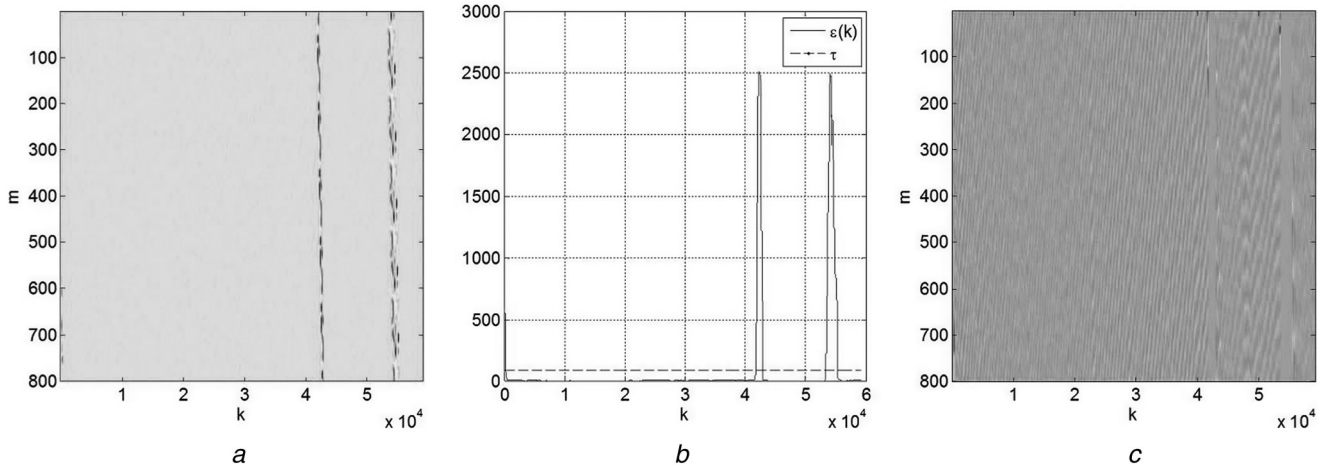

Fig. 6 *Trajectory matrix* $\boldsymbol{Y}$*, corresponding to the signal*

a Before artefact filtering
b Norm $\varepsilon(k)$ of columns and threshold value τ
c Filtered trajectory matrix $\tilde{\boldsymbol{Y}}_{\mathrm{d}}$ after thresholding operation

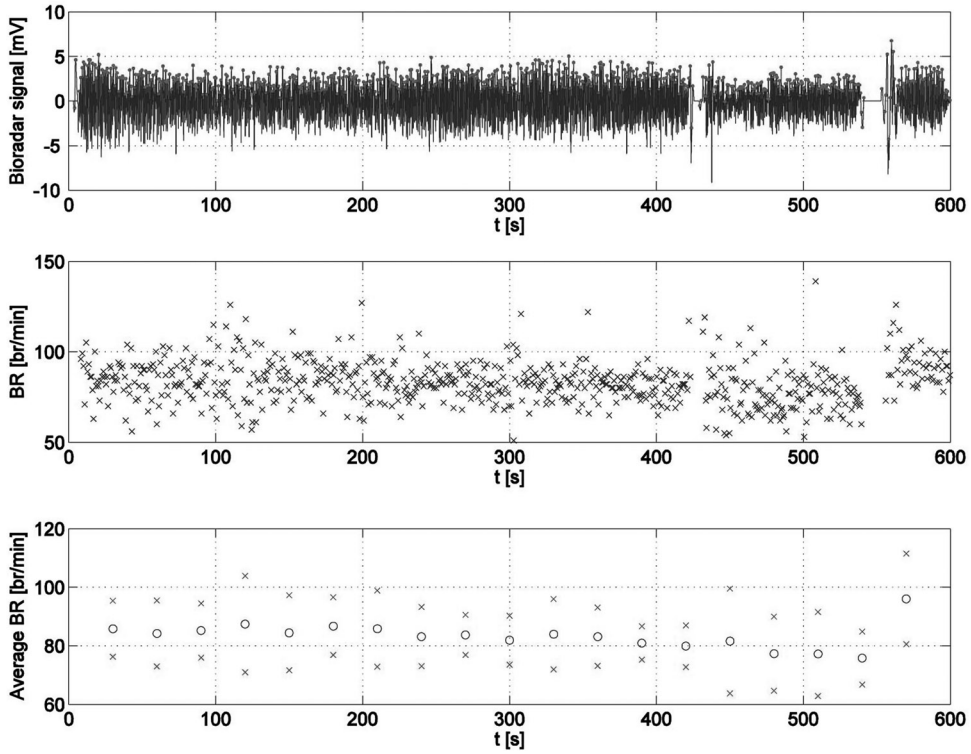

Fig. 7 *Results of signal processing for rat 1. Top panel: filtered radar signal (solid line) and its peaks (symbols). Middle panel: breathing rate. Bottom panel: average breathing rate over a time interval of 30 s (circle) with error bars of one SD (crosses)*

around 0, 430, and 550 s, where strong artefacts are visible (see arrows in Fig. 5). These artefacts are originated by sudden movements of the rat during sleep and have been filtered by the procedure outlined in Section 4. In particular, for the embedding procedure, the length of the mobile window $w(n)$ has been fixed to $M = 800$ signal samples, that is, 8 s.

The trajectory matrix $\boldsymbol{Y}$, corresponding to the signal in Fig. 5, is reported in Fig. 6 and clearly shows an irregular structure due to motion artefacts, which manifest as anomalies along columns. The energy of the columns $\varepsilon(k)$ is depicted in Fig. 6*b* together with the threshold value τ. As foreseen in Section 4, $\varepsilon(k)$ peaks in correspondence of the time intervals containing artefacts, otherwise it is always lower than the threshold τ.

After thresholding, the filtered trajectory matrix $\tilde{\boldsymbol{Y}}_{\mathrm{d}}$ is obtained as seen in Fig. 6*c*. Such a matrix has a much more regular and uniform structure than $\boldsymbol{Y}$ suggesting the rejection of motion artefacts. This expectation is confirmed by the results reported in the top panel of Fig. 7, concerning the filtered signal (solid line) and the estimated peaks (symbols). It can be recognised that the signal has been completely suppressed in time intervals containing motion artefacts. On the basis of the peak locations, the breathing rate of rat 1 has been evaluated and the obtained results are represented in the middle panel of Fig. 7. According to these results, the respiration frequency is not constant over the time but fluctuates approximately between 60 and 100 breaths/min. In order to attain the data to interpret easily, the average breathing rate has been evaluated over time windows of 30 s (as it is usually done for human sleep records), and the corresponding results are plotted in the bottom panel of Fig. 7 together with error bars (crosses) corresponding to one standard deviation (SD). The average breathing rate oscillates around 83 breaths/min. It turns out that the estimated breathing rates are fully compatible with biological information available in the literature. Indeed, the respiratory rate of rats is in the range of 70–100 breaths/min [26].

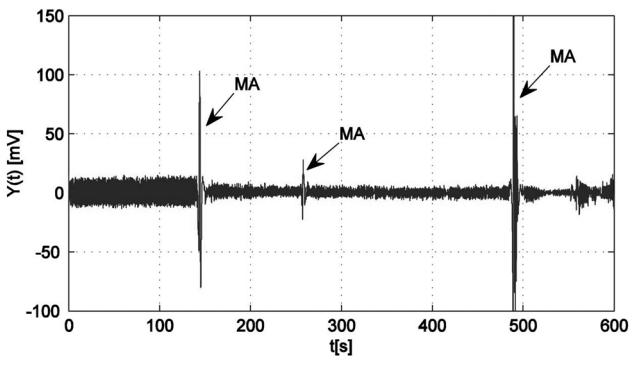

Fig. 8 *Signal at the output of the low-pass filter over the time window [0, 600] s for rat 2. Black arrows denote motion artefacts*

To corroborate the effectiveness of the bioradar device, we report in Figs. 8 and 9 the results of the record for rat 2, which has been collected in the same experimental conditions and is also characterised by motion artefacts. Biologically consistent results are observed also in this case as for all records not included in this work.

It is interesting to compare the signal processing results for rats 1 and 2 (see Figs. 7 and 9). The breathing patterns are remarkably different since the average respiration frequency for rat 1 is about 83 ± 10 breaths/min (mean $\pm$ SD), while the same parameter is about 100 ± 11 breaths/min (mean $\pm$ SD) for rat 2. These differences are caused by individual physiological features of rodents and may be used for distinguishing between different subjects as it is currently done for humans [27].

Most notably, the experimental results showed that it is not only possible to estimate the respiration frequency of sleeping rat by means of the proposed technique, but also to detect slight changes in respiration pattern, for example, hypopnea episodes (see Fig. 10), which in case of frequent repetitions (>15 events/min) may indicate the presence of sleep breathing disorders. However, in our experiments, we detected less than three hypopnea episodes per 30 min for all records, thus it was proved that rats under examination had no such sleep disorders.

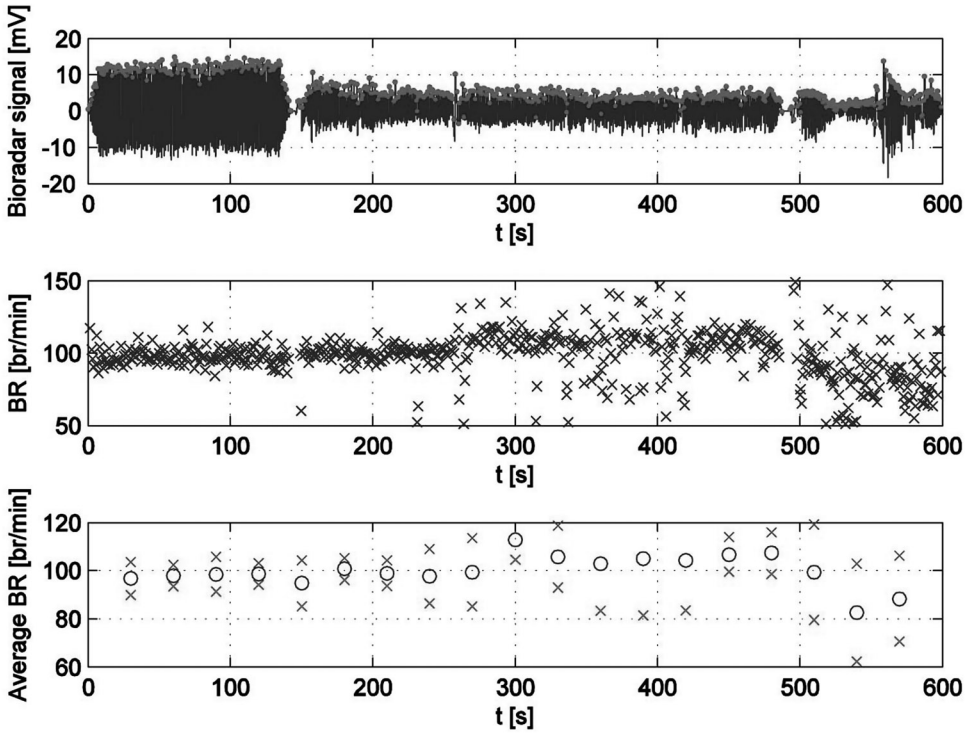

Fig. 9 *Results of signal processing for rat 2. Top panel: filtered radar signal (solid line) and its peaks (symbols). Middle panel: breathing rate. Bottom panel: average breathing rate over a time interval of 30 s (circle) with error bars of one SD (crosses)*

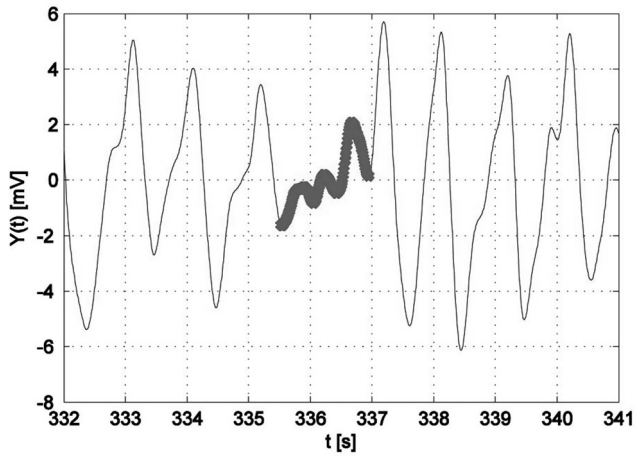

Fig. 10 *Signal from Fig. 8 for rat 2 over the interval [332, 341] s. The hypopnea episode is shown in bold*

6 Conclusion

This work has presented a feasibility study on the monitoring of rodents' breathing activity based on a CW Doppler radar. The experiments have been conducted in laboratory on sleeping rats whose breathing rate has been evaluated contactless by means of an *ad-hoc* developed signal processing strategy. This last has been mainly focused on the filtering of motion artefacts. The effectiveness of the system (hardware plus software) as a tool for a long-term monitoring of breathing rodents activity has been tested. The computational cost is suitable to make the processing in real time, for example, in few seconds after data collection. The results of this study suggest the application of bioradiolocation in realistic operative conditions. The future activity will be directed towards the monitoring of rodents under drug administration and the comparison between medicated versus non-medicated rodents. The bioradiolocation will be validated by exploiting standard clinical instrumentation. This activity will be carried out in cooperation with medical researchers of Sechenov Institute of Evolutionary Physiology and Biochemistry of the Russian Academy of Sciences (Saint-Petersburg, Russia).

7 Acknowledgments

This research has been performed in the framework of the 'Active and Passive Microwaves for Security and Subsurface imaging (AMISS)' EU 7th Framework Marie Curie Actions IRSES project (PIRSES-GA-2010-269157), grant of the President of Russian Federation (MK-889.2014.9) and of Russian Foundation for Basic Research (#15-07-01510A).

8 References

1 Lin, J.C.: 'Non-invasive microwave measurement of respiration', *Proc. IEEE*, 1975, **63**, (10), pp. 557–565
2 Lin, J.C.: 'Microwave apexcardiography', *IEEE Trans. Microw. Theory Tech.*, 1979, **27**, pp. 618–620
3 Boric-Lubecke, O., Lin, J., Park, B.-K., *et al.*: 'Battlefield triage life signs detection technique'. Proc. SPIE Defence and Security Symp., Vol. 6947 – Radar Sensor Technology XII, No. 69470J, Orlando, USA, March 2008, pp. 1–10
4 Greneker, E.F.: 'Radar sensing of heartbeat and respiration at a distance with applications of the technology'. Proc. IEE RADAR-97, Edinburgh, UK, October 1997, pp. 150–153
5 Droitcour, A., Lubecke, V., Lin, J., *et al.*: 'A microwave radio for Doppler radar sensing of vital signs'. Proc. IEEE MTT-S Int. Microwave Symp., Phoenix, USA, May 2001, pp. 175–178
6 Chen, K.M., Huang, Y., Shang, J., *et al.*: 'Microwave life detection systems for searching human subjects under earthquake rubble or behind barrier', *IEEE Trans. Biomed. Eng.*, 2000, **27**, (1), pp. 105–114
7 Bimpas, M., Paraskevopoulos, N., Nikellis, K., *et al.*: 'Development of a three band radar system for detecting trapped alive humans under building ruins', *Prog. Electromagn. Res.*, **49**, 2004, pp. 161–188
8 Holzrichter, J.F., Burnett, G.C., Ng, L.C., *et al.*: 'Speech articulator measurements using low power EM-wave sensors', *J. Acoust. Soc. Am.*, 1998, **103**, (1), pp. 622–625
9 Staderini, E.M.: 'UWB radars in medicine', *IEEE AESS Syst. Mag.*, 2002, **17**, pp. 13–18

10 Kelly, J.M., Strecker R.E., Bianchi, M.T.: 'Recent developments in home sleep-monitoring devices', *ISRN Neurology*, 2012, **2012**, Article ID 768794, pp. 1–10
11 Anishchenko, L., Alekhin, M., Ivashov, S., *et al*.: 'Bioradiolocation: methods and applications', in Pham, T.D., *et al*. (Eds.): 'Biomedical Informatics and Technology' (Springer, Heidelberg, 2014), vol. 404, pp. 10–28, CCIS
12 Li, C., Lin, J.: 'Microwave noncontact motion sensing and analysis' (Wiley, 2014)
13 Immoreev, I.Y.: 'Practical applications of UWB technology', *IEEE Aerosp. Electron. Syst. Mag.*, 2010, **25**, (2), pp. 36–42
14 Wang, J., Wang, X., Zhu, Z., *et al*.: '1D microwave imaging of human cardiac motion: an ab-initio investigation', *IEEE Trans. Microw. Theory Tech.*, 2013, **61**, (5), pp. 2101–2107
15 Kropveld, D., Chamuleau, R.: 'Doppler radar devise as a useful tool to quantify the liveliness of the experimental animal', *Med. Biol. Eng. Comput.*, 1993, **31**, pp. 340–342
16 Anishchenko, L.N., Ivashov, S.I., Vasiliev, I.A.: 'A novel approach in automatic estimation of rats' loco-motor activity'. Proc. SPIE 9077, Radar Sensor Technology XVIII, 90771M, Baltimore, USA, May 2014, pp. 1–8
17 Zeng, T., Mott, C., Mollicone, D., *et al*.: 'Automated determination of wakefulness and sleep in rats based on non-invasively acquired measurement and respiratory activity', *J. Neurosci. Methods*, 2012, **204**, pp. 276–287
18 'Buxco respiratory products'. Available at http://www.datasci.com/products/buxco-respiratory-products, accessed November 2014
19 Oxymax Lab animal monitoring system: CLAMS'. Available at http://www.colinst.com/brief.php?id=61, accessed November 2014
20 'PhenoMaster/LabMaster'. Available at http://www.tse-systems.com/products/behavior/home-cage/phenomaster/ index.htm, accessed November 2014
21 Li, C., Lubecke, V.M., Boric-Lubecke, O., *et al*.: 'A review on recent advances in Doppler radar sensors for noncontact healthcare monitoring', *IEEE Trans. Microw. Theory Tech.*, 2013, **61**, (5), pp. 2046–2060
22 Droitcour, A.D., Boric-Lubecke, O., Lubecke, V.M., *et al*.: 'Range correlation and I/Q performance benefits in single-chip silicon Doppler radars for noncontact cardiopulmonary monitoring', *IEEE Trans. Microw. Theory Techn.*, 2004, **52**, (3), pp. 838–848
23 Park, B.K., Boric-Lubecke, O., Lubecke, V.M.: 'Arctangent demodulation with DC offset compensation in quadrature Doppler radar receiver systems', *IEEE Trans. Microw. Theory Tech.*, 2007, **55**, (5), pp. 1073–1079
24 Vander Vorst, A., Rosen, A., Kotsuka, Y.: 'RF/microwave interaction with biological tissues'. (John Wiley & Sons, 2006) Vol. 181
25 Golyandina, N., Nekrutkin, V., Zhigljavsky, A.: 'Analysis of time series structure: SSA and related techniques' (Chapman and Hall/CRC, 2001)
26 Van Zutphen, L.F.M., Baumans, V., Beynen, A.C.: 'Principles of laboratory animal science' (Elsevier Science, Amsterdam, 2001, 2d edn.)
27 Liu, L., Liu, Z., Barrowes, B.E.: 'Through-wall bio-radiolocation with UWB impulse radar: observation, simulation and signal extraction', *IEEE J. Sel. Top. Appl. Earth Obs. Remote Sens.*, 2011, **4**, (4), pp. 791–798